



Novel Hollow Re-entrant Structures Improving Hydrophobicity of Metal Surfaces

Zhaoqiang Zou^{1,2} · Jinkai Xu^{1,2} · Wanfei Ren^{1,2}

Received: 4 December 2022 / Revised: 9 March 2023 / Accepted: 13 March 2023
© The Author(s) 2023

Abstract

Re-entrant structures have drawn increasing attention because of their hydrophobicity. However, it is very difficult to manufacture re-entrant structures at the micron scale on metal surfaces. In this study, we designed and manufactured novel hollow re-entrant structures employing laser ablation and electrodeposition technology. This designed hollow re-entrant structure on metal surfaces has been fabricated successfully, which has high processing efficiency and good repeatability. The morphology and size of the hollow re-entrant structures were characterized. We found that the hydrophobic performance of hollow re-entrant structures was improved after being in the atmosphere for 3 days. After electrodeposition, the static contact angle was 133°. However, after being placed in the atmosphere for 3 days, the static contact angle was 140.4°, which is 5.2% higher than that after electrochemical deposition. We explained the cause of this phenomenon. The change of element content on the surface of hollow re-entrant structures was used to indicate the formation of metal oxide. After being in the atmosphere for 3 days, oxygen content increased by 0.4%. The metal surfaces with hollow re-entrant structures have a broader application prospect.

Highlights

1. The novel hollow re-entrant structures were designed and fabricated on metal surfaces employing laser ablation and electrodeposition technology.
2. The novel hollow re-entrant structures can effectively improve the hydrophobicity of metal surfaces.
3. The hollow re-entrant structures array can be manufactured in a large area with high efficiency.

Keywords Hollow re-entrant structures · Electrodeposition · Hydrophobic surface

1 Introduction

With the continuous innovation of advanced processing technology, more researchers have paid close attention to hydrophobic surfaces owing to their special wettability. This characteristic can not only result in the material's excellent

water resistance but also has broad application prospects in the fields of self-cleaning [1–3], anticorrosion, anti-icing [4], and oil–water separation [5–7]. However, the rough hierarchical structures and low-surface-energy components of hydrophobic surfaces are unstable. In general, rough hierarchical structures and low-surface-energy components are easily destroyed under a slight shear force, resulting in a performance loss which has become the prominent barrier hindering the practical applications of hydrophobic surfaces. Therefore, developing new hydrophobic surface structures and preparation methods is urgent.

The preparation methods of hydrophobic surfaces, such as laser ablation [8], soft transfer [9], nanoimprint lithography [10], photolithography [11], reactive ion etching [12], and micro moulding [13], have been widely explored.

✉ Jinkai Xu
xujinkai2000@163.com

¹ Ministry of Education Key Laboratory for Cross-Scale Micro and Nano Manufacturing, Changchun University of Science and Technology, Changchun 130022, China

² School of Mechanical and Electrical Engineering, Changchun University of Science and Technology, Changchun 130022, China

Luo et al. employed laser ablation technology to manufacture micropatterns on substrates. Amorphous carbon films were deposited via magnetron sputtering technology to achieve the hydrophobicity of a steel surface. However, the amorphous carbon film on a metal surface could easily be damaged [14]. Bae et al. [15] proposed a direct, one-step method to fabricate dual-scale superhydrophobic metal surfaces using wire electrical discharge machining. Microscale sinusoidal patterns with wavelengths of one-hundredth of a micrometer and secondary roughness of pits were prepared. However, this method is limited by processing materials and cannot be widely employed. In recent years, laser ablation and electrodeposition have been increasingly applied in fabricating metal hydrophobic surfaces. Laser ablation was used to prepare microgrooves. Subsequently, electrodeposition was used to prepare micro-nano structures on the microgrooves [16]. Kwon et al. [17] prepared superhydrophobic metal surfaces via laser ablation and electrodeposition. Re-entrant structures and surface roughness are essential in fabricating superhydrophobic surfaces on intrinsic hydrophilic materials. Liu et al. employed 3D printing technology to manufacture micro re-entrant structures and achieved programmable liquid bonding. However, the manufacturing efficiency of this method was low [18]. Han et al. [19] employed the novel “top-down” and “bottom-up” hybrid methods consisting of ultrafast laser ablation and chemical bath treatment to prepare 3D re-entrant CuO nanograin layered surfaces on Cu microcones. However, the repeatability of re-entrant structures manufactured by this method is poor. Song et al. manufactured micro-reentrant structures applying electrodeposition technology by adjusting the shape of the liquid–gas interface. But the control process of adjusting the shape of the liquid–gas interface is complicated [20]. The previous research results illustrated that the combination of

laser ablation and electrodeposition significantly affects the preparation of hydrophobic metal surfaces.

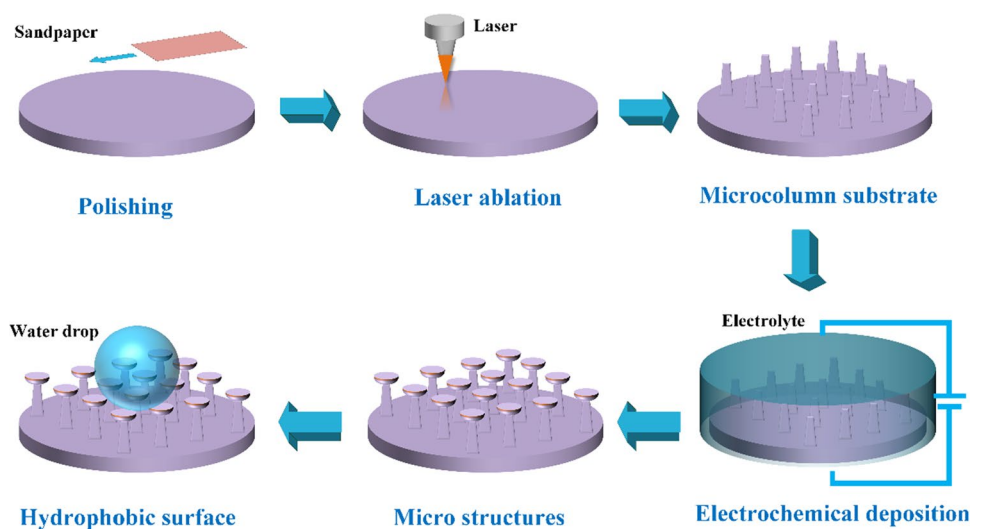
In this study, we designed a hollow re-entrant structure, which can be manufactured through laser-assisted electrochemical deposition on a metal surface to improve its hydrophobicity. Compared to the methods mentioned above, this method has the advantages of cheaper equipment, easier operation, and lower energy consumption. Moreover, it does not require complicated control steps and is similar to a simple electroplating process. However, the repeatability of hollow re-entrant structures is excellent, which is essential for broad applications [17, 20]. First, laser ablation fabricated microcolumns with a wide bottom and narrow top. It was unlikely that CuSO_4 solution would completely flow into the gap because of the close distance between microcolumns. Then, hollow re-entrant microstructures were fabricated by electrodeposition technology and the tip effect ensured that copper was deposited at a specified position. Finally, we characterized the morphology and element composition of hollow re-entrant microstructures. The hydrophobicity of the metal surface was tested immediately and after being placed in the air for 3 days.

2 Experimental

2.1 Experiment Details

Commercial copper plates were used to prepare micropillar arrays. The diameter of the round copper sheet was 15 mm, which can fit the electrode clamp accurately. Acetone solution and #2000 sandpaper were used in the first step. An electrolyte containing $1 \text{ mol L}^{-1} \text{ CuSO}_4$ solution was used in electrodeposition.

Fig. 1 The flowchart of manufacturing steps of hollow re-entrant structures on a metal surface



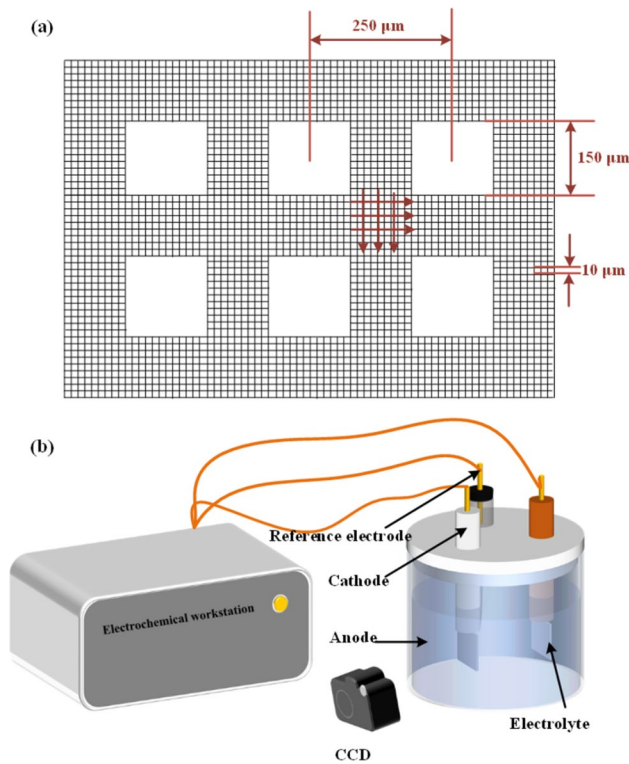


Fig. 2 a Fabrication of laser spot trajectory of microcolumn array. b Typical three-electrode electrochemical deposition system

The systematic preparation process of hydrophobic surface structures is mainly divided into the following parts, as shown in Fig. 1. The copper substrate was polished with sandpaper to remove the uneven surface and make it as smooth as a mirror. Then, the copper substrate was cleaned by ultrasound and then dried. Then, the substrate with a microcolumn array was prepared by laser ablation with a nanosecond laser. The edges and angles of the microcolumn array structures were significantly observed. Substrates were then supersonically washed in acetone solution for 300 s to remove surface impurities and then dried. The most important step is electrodeposition technology. The formation of microstructures mainly utilized the tip effect in electrodeposition process, which can control the reduction of copper ions at the four edges on the microcolumn to form metal copper.

Figure 2 depicts the pre-designed laser spot trajectory of laser etching (Fig. 2a) and a typical three-electrode electrochemical deposition system (Fig. 2b). The solid line represents the laser processing area in Fig. 2a. The scanning interval was set to 10 μm to ensure that the material between the two lines could also be removed. The non-processing area was a square with a side length of 150 μm and a center

distance of 250 μm. The final hollow re-entrant structures were manufactured by using the tip effect of electrodeposition. The typical three-electrode electrochemical deposition system (Fig. 2b) included a charge-coupled device (CCD) camera, an electrochemical workstation, an electrolyte container, and a copper anode (99.99% purity, 1.5 mm in diameter). The distance between the anode and cathode was at a certain value. The CuSO_4 solution was employed as the raw material. The reaction phenomenon was observed using a CCD camera.

2.2 Characterization

To represent the results of this research method, the features of the 3D structure morphology were characterized using a scanning electron microscope (SEM) (Zeiss, EVO 20, Germany). The surface roughness and structural characteristics can be observed in detail. In addition, the height detail was captured by a confocal laser scanning microscope (LSM) (ZEISS, LSM700, Germany). In particular, comparing the size characteristics of the microstructures after laser ablation and electrodeposition under different parameters was convenient.

3 Results and Discussion

3.1 Study on Processing Parameters for Fabricating the Substrate

In order to promote the re-entrant structures more accurately, the parameters of laser ablation must be further specified. A nanosecond laser processing system is adopted. The laser parameters are 1064-nm wavelength, 10-μm spot diameter, and 100-ns pulse width. The temperature and energy of the laser have an approximate Gaussian spatial distribution. Hence, the temperature and energy were maximum at the center of the spot and minimum at the edge. The removal rate of the base material is significantly affected by temperature and energy. To be specific, the removal rate of the substrate is positively correlated with temperature and energy [21, 22]. Therefore, the microcolumns manufactured via laser ablation were subulate [23]. The impact of laser parameters on the geometric dimensions of microcolumns was investigated in detail. As depicted in Fig. 2a, the microcolumn array with a center distance of 250 μm was manufactured by laser spot scanning the pre-designed scanning path. By adjusting laser parameters, microcolumn arrays were fabricated on copper substrates. The unique surface morphology provided great advantages for electrodeposition in the next step.

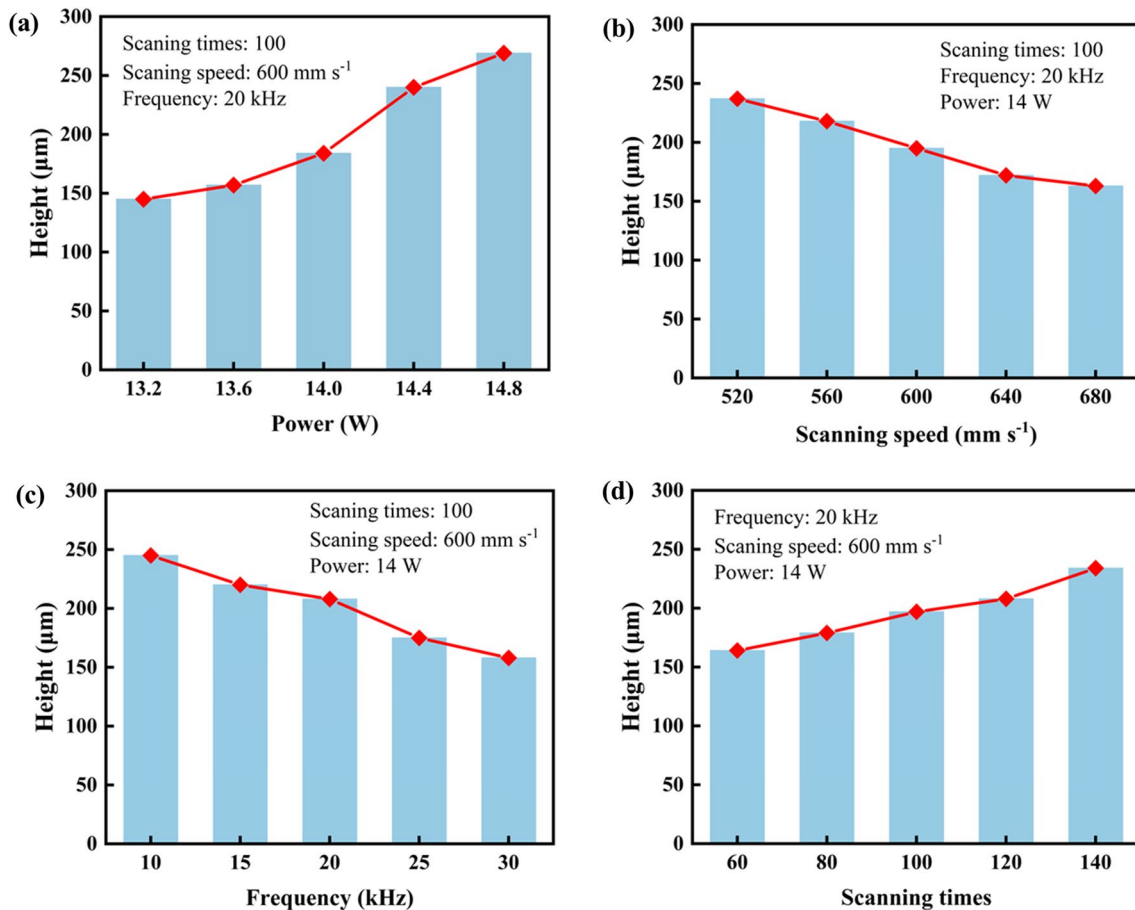


Fig. 3 Influence of laser parameters on the microcolumn height. **a** The influence of laser power on microcolumn height. **b** The influence of laser scanning speed on microcolumn height. **c** The influence

of laser frequency on microcolumn height. **d** The influence of laser scanning times on microcolumn height

The metallic material can be ablated when the laser irradiation temperature is greater than the melting point of materials [21]. Furthermore, the temperature of radiation region is determined by the energy density of laser. Thus, with the continuous removal of material volume, the height characteristics of microcolumns are gradually clear. The impacts of laser parameters used in the experiment on the morphology change of microcolumn are shown in Fig. 3. Also as shown in Fig. 3a, the scanning speed was set to 600 mm/s, the number of scanning was set to 100, and the frequency was set to 20 kHz, the height of microcolumn changes with laser power. Owing to higher laser energy resulting in a fast material removal speed, the height of microcolumn almost increased linearly with the increase in laser power. The height of the microcolumn increased from 145 to 269 μm as the power increased from 13.2 to 14.8 W. When the power was set to 14 W, the frequency was set to 20 kHz and the

scanning times was set to 100, the change of microcolumn height with the scanning speed is shown in Fig. 3b. The height of microcolumn gradually decreased from 237 to 163 μm with the increase of the scanning speed from 520 to 680 mm/s. The variation of the height with the frequency at a scanning speed of 600 mm/s, power of 14 W, and scanning times of 100 was illustrated in Fig. 3c. The height slowly decreased from 245 to 158 μm as the frequency increased from 10 to 30 kHz. The variation of the height with the scanning times at a power of 14 W, scanning speed of 600, and frequency of 20 kHz is demonstrated in Fig. 3d. The height increased from 164 to 234 μm as the scanning times increased from 60 to 140. By comparing the manufacturing quality of microcolumns under different parameters, the following optimal parameters were obtained: scanning times (100), laser power (14 W), scanning speed (600 mm s⁻¹), and pulse frequency (20 kHz).

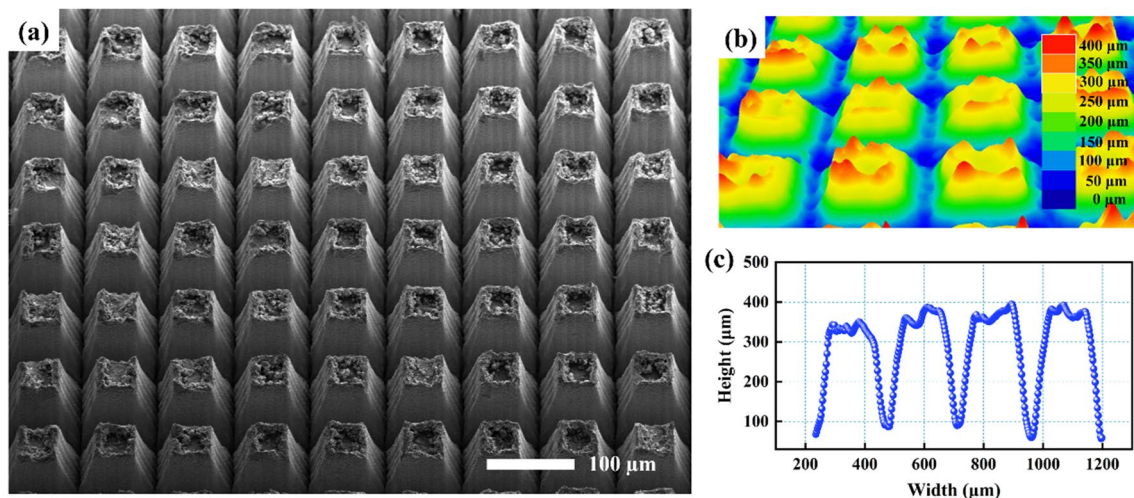


Fig. 4 **a** Morphology of the microcolumn array fabricated under a scanning speed of 600 mm s^{-1} , power of 14 W, frequency of 20 kHz, and scanning time of 100. **b** Image of the microcolumn captured by

a confocal laser scanning microscope (LSM). **c** Outline drawing of microcolumns

Figure 4 depicts the morphology of the microcolumn array manufactured under the condition of 600 mm s^{-1} scanning speed, 14 W power, 20 kHz frequency, and 100 scanning times. Figure 4a shows that after the laser ablation, the microcolumn displayed a high degree of consistency, showing a narrow upper and wide lower structural morphology. This outcome can be explained by the uneven energy distribution of the laser spot, which led to the difference in the material removal rate. The existence of the laser thermal effect made the edge of the microcolumn upper surface produce a recast layer, which was essential to this study. Owing to the edge effect, it provided a basis for the subsequent preparation of re-entrant structures. The structure of the recast layer is presented in Fig. 4b. Figure 4c shows the microcolumn outline drawing. The width of the upper surface of the microcolumn was approximately $100 \mu\text{m}$, which was consistent with the designed size in Fig. 2a.

3.2 Effect of Deposition Potential and Deposition Time on Hollow Re-entrant Structures

Hollow re-entrant structures were prepared by electro-deposition, which employed the designed microcolumn array (Fig. 4a) as the deposition substrate in the second step. Subsequently, large-area re-entrant structures were manufactured on the metal surface. The influence of electro-deposition parameters on the geometric dimensions of the re-entrant structures was thoroughly studied. Figure 5a depicts the SEM images of the re-entrant structures obtained

under the deposition potentials from -0.70 to -0.85 V and deposition times from 300 to 900 s in $1 \text{ mol L}^{-1} \text{ CuSO}_4$ electrolyte. The results show that the height of the deposition layer at the upper edge of the microcolumns was higher than that at the center, forming hollow re-entrant structures. It is found that copper deposition was observed at the edge of microstructures. There was almost no copper deposition between microstructures, regardless of the deposition potential. In this study, when the deposition time was very short, such as 300 s, the re-entrant structures were not apparent even when the deposition potential was very high (-0.9 V). However, the basic outline of re-entrant structures could be observed by SEM picture when the deposition time was prolonged to 600 s. Therefore, the size of re-entrant structures could be adjusted by adjusting the deposition time. When the deposition time was 900 s, the re-entrant structures could be observed clearly. The deposition potential is the main factor that determines the deposition rate, which provides the driving force for the reduction of metal ions. When the deposition potential was set to -0.70 V , the shape of the hole in re-entrant structures was close to square, which indicated that the deposition width of the four edges was even-distributed. In addition, when the deposition potential was set to -0.75 V and -0.80 V , the current density was higher and the deposition rate was faster. The larger deposition volume resulted in a smaller size of the hollow part. When the deposition potential was increased to -0.85 V , the larger current density led to the formation of powder copper. The deposition of bulk copper

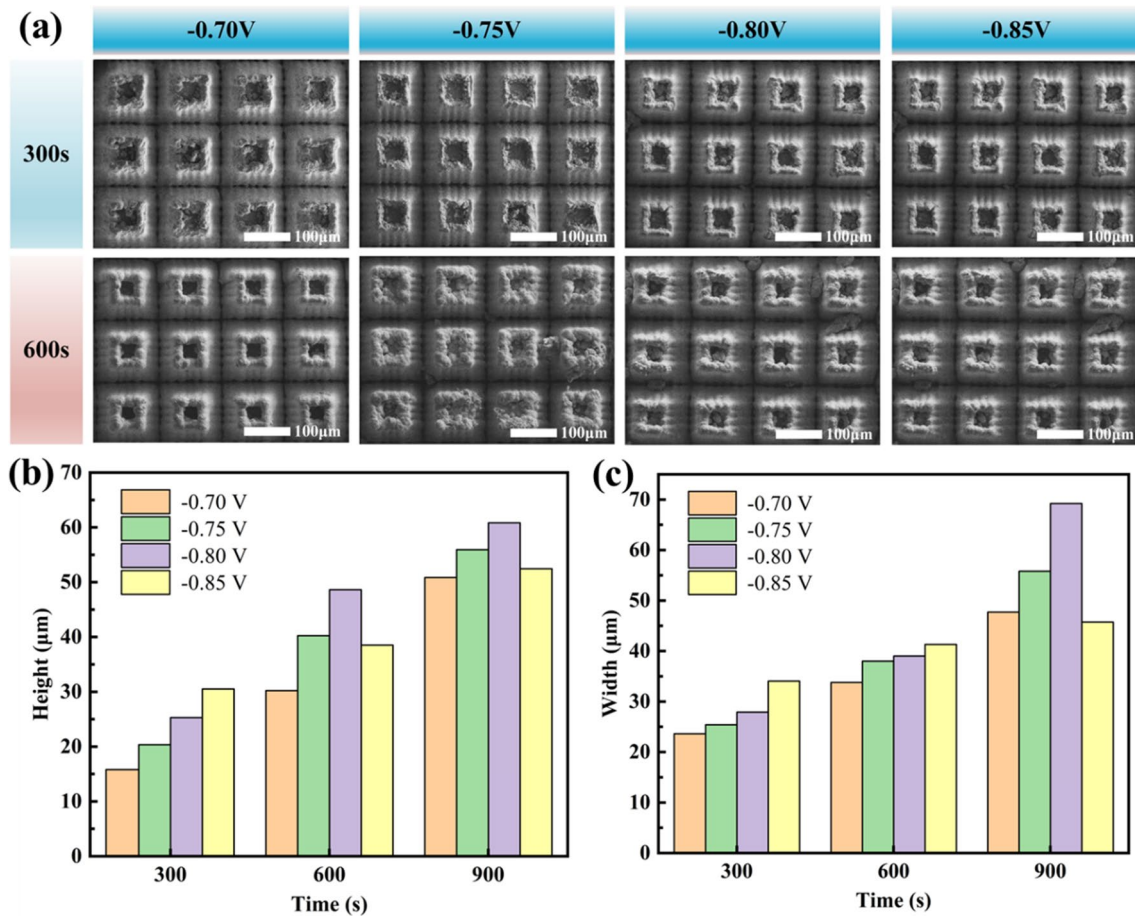


Fig. 5 **a** SEM images of hollow re-entrant structures fabricated under potentials of -0.70 , -0.75 , -0.80 , and -0.85 V and deposition times of 300 and 600 s in a 1 mol l^{-1} CuSO_4 electrolyte. **b** Variation of the

height of the hollow re-entrant structures with time at different deposition potentials. **c** Variation of the width of the hollow re-entrant structures with time at different deposition potentials

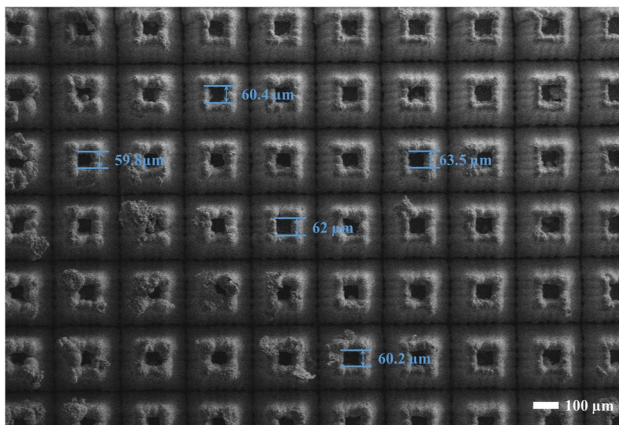


Fig. 6 The measurement of hole size in hollow re-entrant structures

was inhibited, so it was observed that the width of re-entrant structures was smaller than -0.80 V. In this case, there is no linear relationship between the width of microcomponents

and deposition voltage. However, a positive linear correlation exists between deposition width and deposition time at this potential, as shown in Fig. 5a. The curve of hollow re-entrant structures' height changing with the deposition time under different potentials is shown in Fig. 5b. At a specific deposition potential, the deposition height increased with an increase of the deposition time. Another factor determining the deposition height is deposition potential. The height increased with the potential from -0.7 to -0.8 V. However, when the potential was -0.85 V, the deposition height was lower than that at -0.8 V. This is because the potential is too negative, resulting in a dendritic copper. The width variation showed the same trend as the height, as shown in Fig. 5c.

In order to better highlight the characteristics of hollow re-entrant structures, the hole size was measured, as depicted in Fig. 6 (under the parameters of -0.70 V and 900 s). The results indicate that the size distribution of most holes was between 55 and 65 μm, which shows that the hollow re-entrant structures had high consistency, and

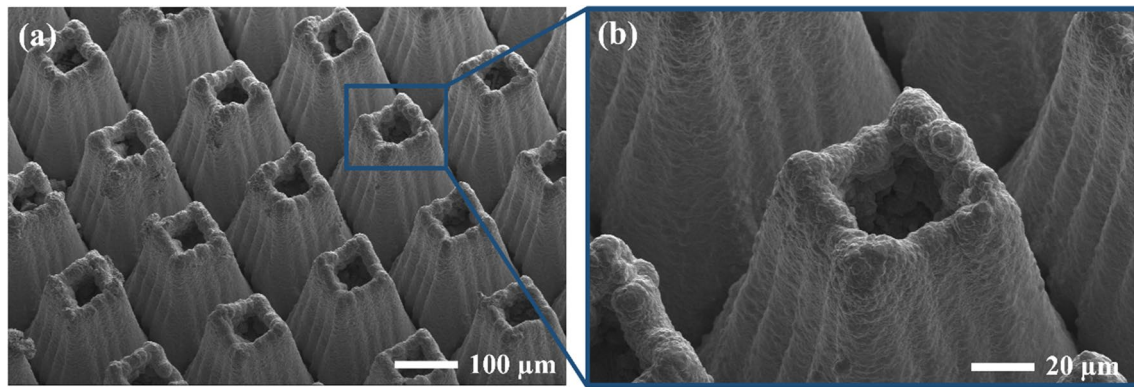


Fig. 7 **a** Re-entrant structures fabricated at -0.70 V and 900 s. **b** The SEM image of a hollow re-entrant structure

there was little difference in deposition rate at each position of the substrate during electrodeposition. By controlling deposition time and deposition potential, hollow re-entrant structures with different pore sizes can be fabricated, which provided a basis for the popularization and application of this method.

The SEM images of the hollow re-entrant structures are shown in Fig. 7. The parameters used to prepare this sample were -0.70 V and 900 s. The re-entrant structures were hollow and showed high consistency. Via electrodeposition, the designed structures can be manufactured in a large area rather than one by one, which greatly improves processing efficiency and reduces costs. Some defects in the structures, such as dendrites, were caused by the high local current density in the electrodeposition process. Therefore, the selection of the electrodeposition parameters is crucial.

3.3 Hydrophobicity Detection of Surface with Re-entrant Structures

3.3.1 Mechanism of Surface Hydrophobicity with Re-entrant Structures

The mechanism of surface hydrophobicity with hollow re-entrant structures can be explained by the Cassie–Baxter model [24, 25]. The diagram of the Cassie–Baxter model is shown in Fig. 8. The contact angle can be calculated by $\cos \theta_r^c = \sigma_s \cos \theta_e + \sigma_s - 1$, where $\cos \theta_r^c$ is the apparent contact angle, θ_e is the equilibrium contact angle on the flat surface, and σ_s is the area fraction of the solid–liquid contact. Re-entrant structures and surface roughness play an important role in the formation of the superhydrophobic surface of the material [17]. After electrodeposition, on the one hand, the space between the re-entrant structures became larger, so when the droplets contacted the metal surface,

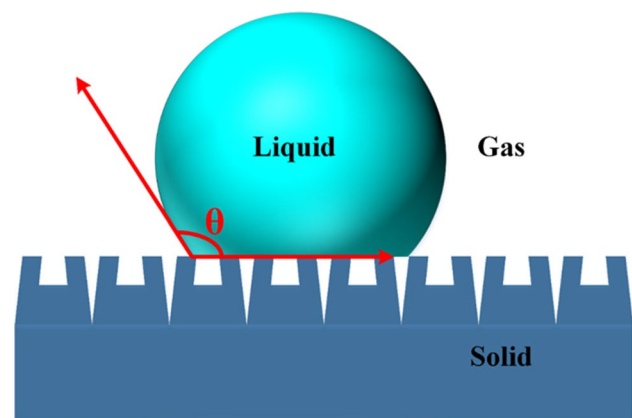


Fig. 8 The schematic diagram of Cassie–Baxter model

most of the air in the hollow re-entrant structures held the droplets. According to the Cassie–Baxter model, the smaller solid–liquid contact area made the larger contact angle. On the other hand, the re-entrant structures made the metal surface roughness relatively larger and improved the hydrophobicity of the metal surface.

The designed hollow re-entrant structures on the copper substrate played an important role in improving the hydrophobicity of the surfaces. To characterize the hydrophobic characteristics of the surfaces, we manufactured several samples. Five samples were fabricated via laser ablation under scanning times of 100, laser power of 14 W, scanning speed of 600 mm s^{-1} , and pulse frequency of 20 kHz. Five samples were prepared via electrodeposition under a potential of -0.70 V. The deposition time was set to 900 s. Figure 9 shows the hydrophobicity test results of the surface manufactured by laser ablation and electrodeposition. After laser ablation, the contact angle values were 113.7° , 117.2° , 109.1° , 113.8° , and 112° without chemical modification. The

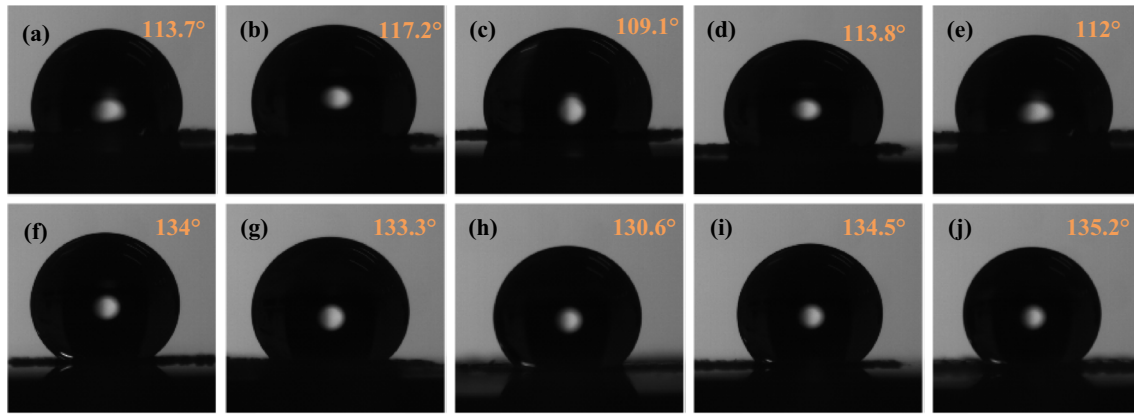
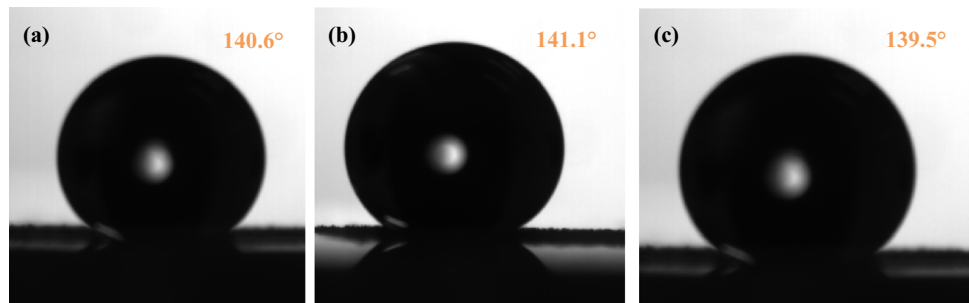


Fig. 9 a–e The hydrophobic angle of five samples after laser processing. f–j The hydrophobic angle of five samples after electrochemical deposition

Fig. 10 The hydrophobic angle of three electrodeposition samples after being placed in the air for 3 days



average weight of the contact angle was 113.16° . After the electrochemical deposition, the contact angle values were 134° , 133.3° , 130.6° , 134.5° , and 135.2° ; the average value was 133.52° . Compared with laser ablation, the contact angle was increased by 18%.

3.3.2 Effect of Elemental Composition on Hydrophobic Properties of Re-entrant Structures Surface

The metal oxides of re-entrant structures have a certain influence on hydrophobic properties [19]. The application environment of the hydrophobic functional surface was generally atmospheric. Therefore, in this study, the surface with hollow re-entrant structures after electrodeposition was placed in the air for 3 days, and then the elemental composition and contact angle were detected, as displayed in Fig. 10. The contact angle values were 140.6° , 141.1° , and 139.5° after being placed in the air for 3 days, the average value reached 140.4° . The value of the contact angle is increased by 5.2% compared with that after electrodeposition. This may be due to the oxidation of copper

element on the surface of re-entrant structures in the air to form nanostructured copper oxide, which improved the hydrophobic characteristics of the surface. In order to explain this phenomenon, the elemental composition of electrodeposition re-entrant structures surface and after being placed in air for 3 days was detected, as depicted in Fig. 11. The surface elements of re-entrant structures were mainly composed of oxygen and copper. The distribution of copper element clearly showed the morphology of microstructures. After electrodeposition, the copper and oxygen element were 98.1% and 1.9%, respectively. Oxygen element was mainly caused by oxygen entering the reaction process when the electrodeposition was carried out in the air environment. After being placed in the air for 3 days, the copper element was 97.7% and oxygen element was 2.3%, where the oxygen content increased by 0.4%. The increase of oxygen content was mainly due to the oxidation of copper in air. Therefore, it was proven that the hydrophobic surface with re-entrant structures has broad application prospects in an air environment.

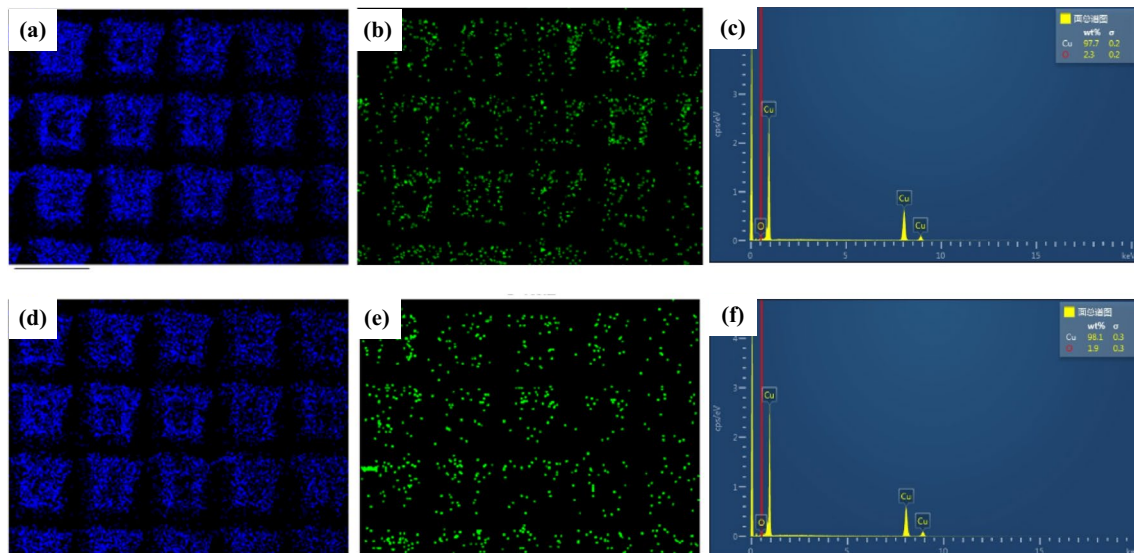


Fig. 11 **a** The EDS map of copper content in re-entrant structures after being placed in the air for 3 days. **b** The EDS map of oxygen content in re-entrant structures after being placed in the air for 3 days. **c** Percentage chart of copper and oxygen content after being placed in

air for 3 days. **d** The EDS map of copper content in re-entrant structures after electrodeposition. **e** The EDS map of oxygen content in re-entrant structures after electrodeposition. **f** Percentage chart of copper and oxygen content after electrodeposition

4 Conclusions

The hydrophobicity of material surfaces is crucial for corrosion prevention and material service life. However, microstructures on metal surfaces can improve surface hydrophobicity. However, for the current technology, it is difficult to prepare hollow re-entrant structures on metal surfaces by one processing technology. In this study, a two-step manufacturing technology was adopted to successfully manufacture the re-entrant structures designed by ourselves and achieve hydrophobic performance. The following two conclusions can be drawn:

- (1) A novel hollow re-entrant structure was designed to improve surface hydrophobicity and prepared by employing laser ablation and electrodeposition technology. The hollow re-entrant structures were fabricated successfully on the copper substrate, which has high processing efficiency and good repeatability. The results show that the size distribution of most holes was between 55 and 65 μm . The average size of the holes was about 61.18 μm . This technology has unique advantages in manufacturing hollow re-entrant structures and broad application prospects.
- (2) The contact angle of samples with hollow re-entrant structures manufactured by this two-step manufacturing technology can reach 133° . However, the contact angle can reach 140.4° after being placed in the air for 3 days. The value of the contact angle is increased by 5.2% compared with that after electrodeposition. The change

of oxygen content in the re-entrant structures shows that copper is oxidized in air and improves hydrophobic characteristics. We speculate that the hydrophobic performance of the surface with re-entrant structures in the air will be greatly improved in a certain period.

Acknowledgements This work was supported by The National Key Research and Development Program of China (2022YFB4600202); Applied Basic Research Project of Key R&D Program of Changchun Science and Technology Bureau (21ZY37); The Fund for the Central Government Guides Local Science and Technology Development Funds to the Special Basic Research of Jilin Province (No. 202002039JC); Jinlin Innovation and Entrepreneurship Talent Funding Project (No. 2021Z002).

Author contributions All authors read and approved the final manuscript.

Availability of Data and Materials The datasets generated during and/or analyzed during the current study are available from the corresponding author upon reasonable request.

Declarations

Conflict of interest The authors declare that they have no conflicts of interest.

Open Access This article is licensed under a Creative Commons Attribution 4.0 International License, which permits use, sharing, adaptation, distribution and reproduction in any medium or format, as long as you give appropriate credit to the original author(s) and the source, provide a link to the Creative Commons licence, and indicate if changes were made. The images or other third party material in this article are included in the article's Creative Commons licence, unless indicated otherwise in a credit line to the material. If material is not included in

the article's Creative Commons licence and your intended use is not permitted by statutory regulation or exceeds the permitted use, you will need to obtain permission directly from the copyright holder. To view a copy of this licence, visit <http://creativecommons.org/licenses/by/4.0/>.

References

- Liu K, Jiang L (2011) Metallic surfaces with special wettability. *Nanoscale* 3:825–838
- Liu Z, Liu H, Li W et al (2022) Optimization of bioinspired surfaces with enhanced water transportation capacity. *Chem Eng J* 433:134568
- Xu K, Ren S, Song J et al (2021) Colorful superhydrophobic concrete coating. *Chem Eng J* 403:126348
- Crick CR, Parkin IP (2010) Preparation and characterisation of super-hydrophobic surfaces. *Chem Eur J* 16(12):3568–3588
- Wang J, Xu J, Chen G et al (2020) Reversible wettability between underwater superoleophobicity and superhydrophobicity of stainless steel mesh for efficient oil–water separation. *ACS Omega* 6(1):77–84
- Pan Y, Liu L, Zhang Z et al (2019) Surfaces with controllable super-wettability and applications for smart oil–water separation. *Chem Eng J* 378:122178
- Chen C, Weng D, Mahmood A et al (2019) Separation mechanism and construction of surfaces with special wettability for oil/water separation. *ACS Appl Mater Interfaces* 11(11):11006–11027
- Nakajima A, Omiya M, Yan J (2022) Generation of micro/nano hybrid surface structures on copper by femtosecond pulsed laser irradiation. *Nanomanuf Metrol* 5(3):274–282. <https://doi.org/10.1007/s41871-022-00135-9>
- Yao J, Wang JN, Yu YH et al (2012) Biomimetic fabrication and characterization of an artificial rice leaf surface with anisotropic wetting. *Chin Sci Bull* 57(20):2631–2634
- Radha B, Lim SH, Saifullah MSM et al (2013) Metal hierarchical patterning by direct nanoimprint lithography. *Sci Rep* 3(1):1–8
- Kwak MK, Jeong HE, Kim T et al (2010) Bio-inspired slanted polymer nanohairs for anisotropic wetting and directional dry adhesion. *Soft Matter* 6(9):1849–1857
- Zhu D, Li X, Zhang G et al (2010) Mimicking the rice leaf from ordered binary structures to anisotropic wettability. *Langmuir* 26(17):14276–14283
- Gao J, Liu Y, Xu H et al (2009) Mimicking biological structured surfaces by phase-separation micromolding. *Langmuir* 25(8):4365–4369
- Luo BH, Shum PW, Zhou ZF, Li KY (2010) Preparation of hydrophobic surface on steel by patterning using laser ablation process. *Surf Coat Technol* 204:1180–1185
- Bae WG, Song KY, Rahmawan Y, Chu CN, Kim D, Chung DK, Suh KY (2012) One-step process for superhydrophobic metallic surfaces by wire electrical discharge machining. *ACS Appl Mater Interfaces* 4:3685–3691
- Hu M, Xu K, Zhang Z et al (2021) Realizing of anisotropic wetting and superhydrophobicity on stainless steel surface by combining picosecond laser ablation and electrodeposition. *Steel Res Int* 92(10):2100119
- Kwon MH, Shin HS, Chu CN (2014) Fabrication of a super-hydrophobic surface on metal using laser ablation and electrodeposition. *Appl Surf Sci* 288:222–228
- Liu X, Gu H, Ding H et al (2019) Programmable liquid adhesion on bio-inspired re-entrant structures. *Small* 15(35):1902360
- Han J, Cai M, Lin Y et al (2018) 3D re-entrant nanoglass on microcones for durable superamphiphobic surfaces via laser-chemical hybrid method. *Appl Surf Sci* 456:726–736
- Song J, Pan W, Wang K et al (2020) Fabrication of micro-reentrant structures by liquid/gas interface shape-regulated electrochemical deposition. *Int J Mach Tools Manuf* 159:103637
- Shuja SZ, Yilbas BS (2011) Laser produced melt pool: influence of laser intensity parameter on flow field in melt pool. *Opt Laser Technol* 43(4):767–775
- Yang Y, Chen Z, Zhang Y (2016) Melt flow and heat transfer in laser drilling. *Int J Therm Sci* 107:141–152
- Cha D, Axinte D, Billingham J (2019) Geometrical modelling of pulsed laser ablation of high performance metallic alloys. *Int J Mach Tools Manuf* 141:78–88
- Patankar NA (2003) On the modeling of hydrophobic contact angles on rough surfaces. *Langmuir* 19(4):1249–1253
- He B, Patankar NA, Lee J (2003) Multiple equilibrium droplet shapes and design criterion for rough hydrophobic surfaces. *Langmuir* 19(12):4999–5003



Zhaoqiang Zou received the Bachelor of Engineering from Changchun University of Science and Technology, Changchun, China, in 2022. He is currently a Ph.D. student in the School of Mechanical and Electrical Engineering in Changchun University of Science and Technology. His current research focuses on Non-traditional machining.



Jinkai Xu is currently a professor in School of Mechanical and Electrical Engineering in Changchun University of Science and Technology. He is also the director of Ministry of Education Key Laboratory for Cross-Scale Micro and Nano Manufacturing. His current research interests include Micro and Nano Manufacturing and Non-traditional machining.



Wanfei Ren received the Ph.D. degree from Changchun University of Science and Technology in 2021. He is a lecturer in School of Mechanical and Electrical Engineering in Changchun University of Science and Technology. His current research focuses on Micro and Nano Manufacturing and Non-traditional machining.